Experimental Evidence on Non-Applicability of the Standard Retardation Condition to Bound Magnetic Fields and on New Generalized Biot-Savart Law

A.L. Kholmetskii

Department of Physics, Belorussian State University
F. Skorina Avenue 4, 220080, Minsk, Belorussia

O.V. Missevitch

Institute of Nuclear Problems, Belorussian State University
Bobruyskaya 11, 220050, Minsk, Belorussia

R. Smirnov-Rueda

Applied Mathematics Department, Faculty of Mathematics
Complutense University, 28040 Madrid, Spain

R.I. Tzontchev, A.E. Chubykalo and I. Moreno

Faculty of Physics, University of Zacatecas
C-580, Zacatecas 98068, ZAC., Mexico

Abstract

In this work we made an analysis of the current status of velocity dependent (bound) field components in the framework of the standard electromagnetic theory. Preliminary discussions of the structure of the magnetic field due to an idealized oscillating magnetic dipole provided us with the quantitative insights on the relative contribution of velocity dependent (bound) and acceleration dependent (radiation) terms into the resultant magnetic field. According to this analysis we defined the methodological scheme based on a generalized (time-dependent) Biot-Savart law capable to test the applicability of the standard retardation condition on bound field components. In the second part of this work we made the theoretical analysis of the finite size multi-section antennas, confirming the validity of the methodological scheme conceived for an idealized magnetic dipole. The use of multi-section antennas is fully justified by a substantial rise of the ratio of bound-to-radiation field strength. Finally, we effected numerical calculations taking into account particular experimental settings and compared them with experimentally obtained data that unambiguously indicate on the non-applicability of the standard retardation condition to bound magnetic fields. In addition, experimental observations show a striking coincidence with the predictions of a new generalized Biot-Savart law which implies the spreading velocity of bound fields highly exceeding the velocity of light.

Key words: *Maxwell's equations, bound field components, retardation constraint, spreading velocity of bound fields, multi-section antenna, zero crossing method*

1 Introduction

Nowadays, the standard classical electrodynamics is perceived as the paradigm of a causal and deterministic classical field theory. The most general approach to the calculation of electric and magnetic fields is explicable in terms of the so-called Lienard-Wiechert potentials. Their conventional form in the case of an arbitrary moving classical point charge of magnitude q is given as[1]−[2]:

$$\varphi = \frac{q}{4\pi\varepsilon_0}\left[\frac{1}{R - \frac{\mathbf{u}\cdot\mathbf{R}}{c}}\right]_{ret} ; \qquad \mathbf{A} = \frac{q}{4\pi\varepsilon_0}\left[\frac{\frac{\mathbf{u}}{c}}{R - \frac{\mathbf{u}\cdot\mathbf{R}}{c}}\right]_{ret} \tag{1}$$

where the corresponding quantity in brackets means that it is evaluated at the retarded time $t' = t - R/c$; R is the distance from the retarded position of the charge to the point of observation and $\mathbf{u}$ is a velocity of a charge at the instant of time t'.

As our intention to make clear the main proposals of this work, we first discuss the fundamental underlying structure of existing solutions. Electric and magnetic field values $\mathbf{E}$ and $\mathbf{B}$ are related to potentials (1) by the equations:

$$\mathbf{E} = -\boldsymbol{\nabla}\varphi - \frac{\partial\mathbf{A}}{\partial t}; \qquad \mathbf{B} = \boldsymbol{\nabla}\times\mathbf{A} \tag{2}$$

Straightforward application of operations (2) performed on (1) provides the standard expression for field strengths of an arbitrary moving point charge[1]−[2]:

$$\mathbf{E} = \frac{q}{(4\pi\varepsilon_0)}\left\{\left[\frac{(\mathbf{n}-\frac{\mathbf{u}}{c})(1-(\frac{\mathbf{u}}{c})^2)}{k^3 R^2}\right]_{ret} + \left[\frac{\mathbf{n}}{k^3 R}\times\left\{\left(\mathbf{n}-\frac{\mathbf{u}}{c}\right)\times\frac{\dot{\mathbf{u}}}{c}\right\}\right]_{ret}\right\} \tag{3}$$

$$\mathbf{B} = [\mathbf{n}\times\mathbf{E}] \tag{4}$$

here $\mathbf{n} = \frac{\mathbf{R}}{R}$ and $k = 1 - \frac{\mathbf{n}\cdot\mathbf{u}}{c}$;.

Both electric $\mathbf{E}$ and magnetic $\mathbf{B}$ fields are composed of two *essentially* different parts:

$$\mathbf{E} = \mathbf{E_u} + \mathbf{E_a}; \qquad \mathbf{B} = \mathbf{B_u} + \mathbf{B_a} \tag{5}$$

where $\mathbf{B_u} = \mathbf{n}\times\mathbf{E_u}$ and $\mathbf{B_a} = \mathbf{n}\times\mathbf{E_a}$.

The first terms $\mathbf{E_u}$ and $\mathbf{B_u}$ are usually regarded as *velocity fields* because they are independent of acceleration $\dot{\mathbf{u}}$. The electric velocity field $\mathbf{E_u}$ falls off as R^{-2} that is the substantial feature of the radial (longitudinal) field components associated with the static Coulomb law. By this reason the velocity fields are also referred as *bound or longitudinal fields*. On the contrary, the second parts of solutions (3)-(4), denoted as $\mathbf{E_a}$ and $\mathbf{B_a}$ are linear functions of acceleration, falling off proportional to R^{-1}. These terms are responsible for the radiation and take no place in the case of uniformly moving charge (as well as at rest), giving priority to bound components in the formation of electromagnetic (EM) field. The latter fact poses a question of considerable fundamental interest concerning the nature and physical characteristics on bound fields. It implies a fundamental question of whether the applicability of the standard retardation condition to all components of electromagnetic field has solid theoretical, methodological and

empirical grounds. Put in other terms, should be there an explicit empirical test of the applicability of the retardation condition to bound field components?

Doubts about the soundness of the conventional treatment of bound fields appear already when one studies the transition between the initial state of rest (or uniform motion) and the subsequent state of acceleration of the charge. The origin of this important insight resides in the belief that a fully consistent approach to classical electrodynamics demands the continuity of electromagnetic phenomena in all situations. This allowable inference was recently explored in[3]. The mathematical analysis of boundary-value problems for D'Alembert and Poisson's equations showed that the present set of solutions to Maxwell's equations does not ensure the continuity in transition between, on one hand, the general case of an arbitrary moving charge and, on the other hand, the static or quasi-static (uniform motion) limits. Independent approach implemented in[4] also unambiguously indicates that the transition between two different states of uniform velocity of a charge via an intermediate state of acceleration results in a type of discontinuity in functional form.

The peculiar historical background of the classical EM theory gives an additional motivation to focus our attention on bound fields. The problem of propagation of EM interactions was the crucial point in choosing appropriate theoretical foundations for classical electrodynamics in the 19th century. By the time Hertz began his experiments in providing evidence in favor of EM waves in air, the set of fundamental solutions to Maxwell's equations did not imply any explicit separation into bound and radiation field components. Only Lorentz's modification of Maxwell's theory (1892) provided Lienard (1898) and Wiechert (1901) with inhomogeneous wave equations. The retarded solutions were found under the retardation constraint which, as it is generally accepted, was just experimentally verified by Hertz in 1888[5]. It gave a rise to the fact that bound and radiation field components of Lienard-Wiechert solutions propagate at the same rate.

Thus, in light of our discussion we can see that Hertz's experiments were not especially thought-out to bring solid empirical grounds on the physical characteristics of bound fields as well as to test the applicability of the retardation constraint on them. In modern retrospective, this uncertainty in respect to bound components might imply some sort of methodological incompleteness in Hertz's experimental approach as it has been recently inferred in[6] and, therefore, any attempt to provide a fuller experimental information on bound fields acquires a fundamental importance in the framework of the classical EM theory. As response to these conceptual questions, in this work we propose *an experimental approach* to velocity (bound) fields to test the applicability of the standard retardation constraint to bound field components.

Recently, Hertz's-type experiment has already been attempted[7] in order to remove above-mentioned uncertainties in respect to electric bound field components. However, no explicit information was obtained as regards to the nature of electric bound fields and the front of the detected signal apparently propagated at the light velocity as it is assumed in the standard EM theory. However, the subsequent analysis showed that there was no preliminary theoretical estimation of the relative contribution of bound and radiation components into the final signal. This estimation is crucial if one takes into account that EM radiation terms fall off as R^{-1} and at large distances predominate,

3

determining the time shift of the signal front measured by oscilloscope. Additionally, the chosen spheroid shape of the receiving antenna used in experimental measurements made it especially unsensitive to the direction of the propagating electric field.

There is also another experimental difficulty connected to the estimation of the relative contribution of bound components when the radiation is very intensive, i.e. for frequencies $\omega > 10^8 \ s^{-1}$. In fact, the intensity of EM radiation rapidly increases with ω, hence hindering the sensitivity of measuring devices in respect to bound fields that fall off as R^{-2}. Contrarily, for the low frequency radiation the time resolution of registration systems decreases considerably and results insufficient to measure any EM signal with due precision. Without such preliminary discussion and analysis, the experimental approach effected in[7] looks rather unreliable. Put in other terms, one can not avoid the preliminary calculation of an optimal range of variations of R and ω in which the experimental treatment of bound fields might be attended with expected precision.

In addition to the feebleness of the effects produces by bound fields that fall off as R^{-2}, there are also several technical circumstances that make direct observation of bound fields an extremely difficult task. All known radiation devices (antennas etc) are designed to enhance the radiation to the utmost, i.e. to reach the maximum value of the ratio of radiation-to-bound field strength. In other words, the use of radiation devices in their traditional form can be rather counterproductive and, therefore, there should be a radically different experimental approach based on a substantial rise of the ratio of bound-to-radiation field strength.

As follows, we shall present an experimental scheme that is methodologically conceived to surmount all above-mentioned technical difficulties and to provide unambiguous explicit information on bound magnetic components. The main idea of our method is based on the analysis of EM field in the plane of the loop antenna with oscillating current. Section 2 is devoted to the underlying idea of how the spreading velocity of bound magnetic fields can be measured in an idealized case. In Section 3 a methodological approach will be described in more details as concerns a particular experimental set-up (described in Section 4) which implements multi-section type of antennas in order to increase the ratio of bound-to-radiation field strenght. Finally, Section 5 presents results of numerical calculations and their comparison with experimental data.

2 The structure of EM field due to an idealized magnetic dipole: introduction into methodology of experimental approach

This Section will be devoted to the illustration of the background of the consistent methodological approach to empirical identification of bound magnetic fields. By analogy with the retarded vector potential $\mathbf{A}$, the magnetic field $\mathbf{B}$ can be determined

4

directly by the standard expression[8]−[9]:

$$B(R,t) = \frac{1}{4\pi\varepsilon_0 c^2} \int \left[\frac{\boldsymbol{\nabla}_s \times \mathbf{J}(r_s)}{R} \right] dV_s \tag{6}$$

as the retarded solution of the corresponding D'Alembert equation:

$$\Delta \mathbf{B} - \varepsilon_0 \mu_0 \frac{\partial^2 \mathbf{B}}{\partial t^2} = -\mu_0 \boldsymbol{\nabla} \times \mathbf{J} \tag{7}$$

where $\mathbf{J}$ is the conduction current density; $\mathbf{B} = \boldsymbol{\nabla} \times \mathbf{A}$ and the quantity placed inside the square bracket in Eq. (6) is measured at the retarded time $t' = t - R/c$.

In the low velocity relativistic limit (i.e. when the velocity of charges is much lower than c but the effect of retardation is still taken into account)[8]−[9], the general solution (6) can be presented in an equivalent form of the line integral as the generalized (time-dependent) Biot-Savart law[8]:

$$\mathbf{B} = \mathbf{B_u} + \mathbf{B_a} = \frac{1}{4\pi\varepsilon_0 c^2} \oint_\Gamma \left\{ \frac{[I]}{R^2} + \frac{\left[\dot{I}\right]}{cR} \right\} \mathbf{k} \times \mathbf{n} dl \tag{8}$$

where $\mathbf{n} = \mathbf{R}/R$; I is the conduction current; $\mathbf{k}$ is the unit vector in the direction of $\mathbf{I}$, i.e. $\mathbf{I} = I\mathbf{k}$ and dl is an infinitesimal element of the loop line Γ.

The generalized (time-dependent) Eq. (8) is exact when the centripetal acceleration of the moving charges is ignored (low velocity approximation) and, as it is demonstrated in[9], can be derived directly, starting with (1) for retarded potentials φ and $\mathbf{A}$. As a consequence, the Eq. (8) has a general applicability to usual electric circuits since the velocity of conduction electrons is always much lower than c. The first term on the right hand side of expression (8) is the classical integral form of the Biot-Savart law when the current I in the circuit Γ is steady (i.e. $\dot{I} = 0$).

The velocity dependent (bound) component $\mathbf{B_u}$ arises from the term proportional to $[I]$ whereas the acceleration field $\mathbf{B_a}$ is due to the $\left[\dot{I}\right]$ term. Traditionally, in the general (time-dependent) case solutions to corresponding D'Alembert equations are found under the retardation constraint applied to the whole electromagnetic field, hence providing the same spreading velocity to bound and radiation fields as it takes place in the standard Eq. (8). In view of overwhelming empirical evidences that radiation components propagate at the velocity of light c, we keep the standard retardation constraint unmodified in respect to acceleration fields $\mathbf{B_a}$. Contrarily, we assume that there is no explicit empirical evidence on the way how bound fields propagate in empty space. Using the underlying structure of the Eq. (8), we are now in a position to deal with bound and acceleration fields separately and to explore a wide range of hypothetic retardation constraints in respect to bound components, i.e. the situation when the spreading velocity of bound fields $\mathbf{B_u}$, denoted as v, varies continuously in the range $v \geq c$. In the context of this

5

hypothesis, Eq. (8) acquires an alternative form:

$$\mathbf{B} = \mathbf{B_u} + \mathbf{B_a} = \frac{1}{4\pi\varepsilon_0 c^2} \int \left\{ \frac{[I]_v}{R^2} + \frac{\left[\dot{I}\right]}{cR} \right\} \mathbf{k} \times \mathbf{n} dl \qquad (9)$$

where the corresponding quantity in square bracket $[I]_v$ means that it is evaluated at the different retarded time $t'_v = t - R/v$.

The introduction of the dissimilar approaches to the treatment of bound and radiation fields adds to the difficulty of its justification in the framework of the conventional classical electrodynamics. The theoretical exploration of this case will conceivably imply the extension of foundations and perhaps the rise of new concepts. One possible justification might be based on the use of a two-parameter Lorentz-like gauge (so-called v-gauge)[10] which leaves original Maxwell's equations unmodified and introduces an arbitrary propagational velocity $v \geq c$ for scalar components of electric field (i.e. they can be identified with bound fields). Recently, v-gauge approach is widely discussed as a possible explanation of apparently superluminal group velocity of evanescent waves[11]. Even though the foundations of the hypothetic distinction of propagational velocities of bound and radiation components remain at present stage unclear, the use of Eq. (9) allows us to conceive a general methodological scheme capable to test the applicability of the standard retardation constraint to bound fields, i.e. the case $v = c$. Certainly, any discrepancy between experimental observations and theoretical predictions based on the condition $v = c$ would not automatically imply the correctness of our hypothesis in form of the Eq. (9) but rather no applicability of the standard retardation constraint to bound fields. In the latter case $v \neq c$, the Eq. (9) can be taken as a first approximation to make theoretical predictions that can be verified by experiment.

For further convenience, let us resort to a certain idealization in our attempt to use the basic equation (9) in a less cumbersome representation, keeping untouched all fundamental features related to the bound and radiation components. By these reasons, we first consider an example of idealized oscillating magnetic dipole given in form of a loop antenna with the radius r. It will be assumed that the magnetic dipole moment $\mathbf{m}$ varies harmonically with time at the angular frequency ω. Then the idealization implies two requirements: (a) the radius of the loop r is considerably smaller than the distance R from the center of the antenna to the point of observation; (b) the wavelength λ of emitted EM radiation greatly exceeds the perimeter of the loop, i.e. $\frac{r}{c} \ll \frac{1}{\omega}$. The second requirement means that at a given frequency ω the magnitude of conduction current has nearly the same value I in all parts of the loop circuit at a present instant of time t. This condition, which is usually regarded as an approximation of *quasi-stationary current*, gives a simple relationship $\mathbf{m} = \Delta S I(t) \mathbf{z}$ between the magnetic dipole moment $\mathbf{m}$ and the conduction current value $I(t)$, where ΔS is the area bounded by the loop and $\mathbf{z}$ is the unit vector perpendicular to the plane of the loop. Notice also that the *quasi-stationary current* approximation remains valid for bound components in the whole range $v \geq c$, i.e. $\frac{r}{v} \ll \frac{1}{\omega}$.

Having assumed the above idealizations, the alternative expression (9) results con-

6

siderably simplified. By analogy with the standard procedure[9] (a reader interested in a full derivation can found it in the Appendix), all contributions into the magnetic field in the plane of an oscillating magnetic dipole are:

$$\mathbf{B}(R,t) = -\frac{\Delta S}{4\pi\varepsilon_0 c^2} \left\{ \frac{[I]_v}{R^3} + \frac{c}{v}\frac{\left[\dot{I}\right]_v}{cR^2} + \frac{\left[\ddot{I}\right]}{c^2 R} \right\} \mathbf{z} \qquad (10)$$

where ΔS is the area bounded by the loop of emitting antenna (EA).

If the standard retardation constraint $v = c$ is applied to all components, Eq. (10) takes the form obtained in the low velocity relativistic limit[9],[12]:

$$\mathbf{B}(R,t) = -\frac{\Delta S}{4\pi\varepsilon_0 c^2} \left\{ \frac{[I]}{R^3} + \frac{\left[\dot{I}\right]}{cR^2} + \frac{\left[\ddot{I}\right]}{c^2 R} \right\} \mathbf{z} = -\frac{\mu_0}{4\pi} \left\{ \frac{[\mathbf{m}]}{R^3} + \frac{[\dot{\mathbf{m}}]}{cR^2} + \frac{[\ddot{\mathbf{m}}]}{c^2 R} \right\} \qquad (11)$$

The first and the second terms in *rhs* of Eq. (10) have the common origin and arise from the bound component $\mathbf{B_u}$. The contribution proportional to R^{-3} is a dynamic counterpart of a steady magnetic field produced by a static magnetic dipole of magnitude $\mathbf{m}$. The R^{-2}-term is due to a finite size of the antenna loop which stipulates the difference in the value of retarded time $t' = t - R/v$ for EM signals out-coming from different segments of the perimeter of EA. In other words, a bound field perturbation emitted from the nearest half-part of the loop arrives at the point of observation before an equivalent signal from the farthest half-part. This retarded time shift leads to the contribution proportional to $\dot{I}$ or $\dot{\mathbf{m}}$ (for a more detailed explanation, see Appendix). The last R^{-1}-term is submitted to the standard retardation constraint $v = c$ and corresponds to the magnetic dipole radiation which falls off as R^{-1}.

Let us now take into consideration a receiving loop antenna (RA) under the set of approximations assumed earlier for the EA. Let us place both EA and RA loops in the same plane xy as it is shown in Fig.1. The origin of the coordinate frame coincides with the center of the EA loop and $\mathbf{R}$ denotes the position-vector of the center of the RA loop. The generation of an electromotive force (e.m.f.) $\varepsilon(t)$ is proportional to the time variation of the magnetic field flux (which is empirically established integral form of the Faraday law):

$$\varepsilon(t) = -\frac{d}{dt} \iint_S \mathbf{B} \cdot \mathbf{z} dS \qquad (12)$$

The time variation of the magnetic field $\mathbf{B}(t)$ in the area of the RA is determined by the frequency of oscillations ω of the conduction current $I(t)$ in the circuit of the EA. If the sizes of both EA and RA are similar in magnitude, then in the approximation of the quasi-stationary current for the EA the wavelength λ of the electromagnetic radiation also greatly exceeds the radius of the RA ($\frac{r}{c} \ll \frac{1}{\omega}$). In other words, the magnetic field

7

B has nearly the same strength in all parts of the surface S bounded by the loop of the RA, so that:

$$\varepsilon(t) = -\frac{dB}{dt} \iint\limits_S dS = \frac{(\Delta S)^2}{4\pi\varepsilon_0 c^2} \left\{ \frac{\left[\dot{I}\right]_v}{R^3} + \frac{c}{v}\frac{\left[\ddot{I}\right]_v}{cR^2} + \frac{\left[\dddot{I}\right]}{c^2 R} \right\} \tag{13}$$

where $\Delta S = \iint\limits_S dS$ is the area bounded by the loop of the RA and $B = \mathbf{B} \cdot \mathbf{z}$ is the component of the magnetic field in **z**-direction.

The second R^{-2}-term disappears in the strong limit $v = \infty$. In this hypothetic case, there is no retardation for bound fields and at the point of observation every perturbation emitted from the nearest half-part of the loop will be counteracted by an equivalent signal from the farthest half-part. Therefore, the *in-plane* geometry shown in Fig.1 should be sensitive to any variation of the parameter v, since it directly affects the value of the second R^{-2}-term.

This fundamental feature allows us to formulate a methodology of a consistent experimental approach to bound magnetic components. Obviously, as it has already been inferred in the Introduction, any practical realization of the above-considered scheme may be accompanied by a number of rather delicate technical difficulties. So, in our approach to idealization of experimental conditions, let us first assume that the current $I(t)$ in the EA oscillates harmonically at the angular frequency ω as $I(t) = -I(0)\cos(\omega t)$. Then, an observer can measure the phase of the e.m.f. $\varepsilon_v(t)$ induced in the RA and compare it with the phase of some reference harmonic signal ε_r. In the following, we shall show how it can be implemented.

In the approximation of harmonic conduction current in the EA, Eq. (10) yields:

$$\varepsilon_v(t) = \frac{(\Delta S)^2 I(0)\omega}{4\pi\varepsilon_0 c^2} \left\{ \frac{\sin\omega(t - R/v)}{R^3} + \frac{\omega\cos\omega(t - R/v)}{vR^2} - \frac{\omega^2 \sin\omega(t - R/c)}{c^2 R} \right\} \tag{14}$$

or using notations $\eta = \omega R/c$ and $\eta_v = \omega R/v$ it can be written as:

$$\varepsilon_v(t) = \frac{(\Delta S)^2 I(0)\omega}{4\pi\varepsilon_0 c^2 R^3} \left\{ \sin(\omega t - \eta_v) + \eta_v \cos(\omega t - \eta_v) - \eta^2 \sin(\omega t - \eta) \right\} \tag{15}$$

Thus, all contributions into the value of the induced e.m.f. $\varepsilon_v(t)$ are functions of R, η and η_v but at large distances R, the radiation term proportional to $\eta^2 \sin(\omega t - \eta)$ predominates. Therefore, the phase of the radiation term $(\omega t - \eta)$ can be taken for the definition of the reference signal $\varepsilon_r(t)$:

$$\varepsilon_r(t) = -\varepsilon_r(0)\sin(\omega t - \eta) \tag{16}$$

If the range of variations $v \geq c$ is assumed, there are two natural limit cases: (1) $v = c$ and (2) $v = \infty$. Considering the first limit, which corresponds to the standard assumption, Eq. (15) takes the form:

$$\varepsilon_{v=c}(t) = \frac{(\Delta S)^2 I(0)\omega}{4\pi\varepsilon_0 c^2 R^3} \left\{ \sin(\omega t - \eta) + \eta \cos(\omega t - \eta) - \eta^2 \sin(\omega t - \eta) \right\} \tag{17}$$

The first subplot in Fig.2 shows the comparison between the signal $\varepsilon_{v=c}(t)$ induced in the RA and the reference signal $\varepsilon_r(t)$, according to their evolution with R and t. In the second subplot of Fig.2 we specify relative contributions of R^{-3}, R^{-2} and R^{-1}-terms and their mutual harmonic phase shifts. It explains why $\varepsilon_{v=c}(t)$ and $\varepsilon_r(t)$ are not synchronized, i.e. there is always a finite time shift Δt between instants when both signals $\varepsilon_{v=c}(t)$ and $\varepsilon_r(t)$ cross a zero line. However, at large distances the radiation R^{-1}-term predominates considerably so that R^{-3}, R^{-2}-terms can be referred only as weak perturbations of the dominant R^{-1}-component. In other words, the signal $\varepsilon_{v=c}(t)$ tends to take the harmonic form proportional to $\eta^2 \sin(\omega t - \eta)$, hence forcing the time shift Δt to vanish at large distances (far field zone).

The same analysis is also applicable in the general case for the whole range of variations of the parameter v, i.e. $v \geq c$. In Fig.3 we show diagrams that correspond to the second hypothetic limit ($v = \infty$). At short distances, there is also clearly visible finite time shift Δt when both signals $\varepsilon_{v=\infty}(t)$ and $\varepsilon_r(t)$ cross a zero line. We remind here that in this limit case the contribution proportional to R^{-2} disappears so that only R^{-3} and R^{-1}-terms can be seen in the second sub-diagram of Fig.3. Moreover, if at distances $R > c/\omega$ the first R^{-3}-term results already negligible in comparison with R^{-1}-term (it will be fulfilled in our experimental conditions) the variation of the time shift $\Delta t(R)$ does not exhibit any oscillations as it is shown in Fig.4. We have thus reached the conclusion that the type of variation of $\Delta t(R)$ is very sensitive to the particular value of the parameter v and hence can be subjected to the empirical test. Further on we shall refer this approach as a *zero crossing method*.

Summarizing the discussion of idealized antennas, we would like to emphasize that the requirements imposed by this approximation are hardly available in real experimental practice. On the one hand, the value of the e.m.f. ε depends essentially on the radius r of the loop antenna because it is proportional to $(\Delta S)^2 \sim r^4$. On the other hand, in order to reach the criteria of the quasi-stationary current approximation, one cannot decrease the radius r without moderation, since the precision of measurements critically depends on the intensity of EA and RA signals. Therefore, there should be a balance between mutually excluding requirements. In our attempt to reduce dependence on the radius of the loop r, we resorted to the help of so-called multi-section antennas. As we will show in the next Section, the approximation of *quasi-stationary current* and the maximum ratio of bound-to-radiation field strength can be easily implemented for finite size multi-section antennas (even in the range of high frequencies ω), keeping valid the approach based on the zero crossing method.

3 Methodology of experiment in the case of multi-section antennas

In this Section we shall discuss the methodology of experimental approach to bound fields in the case of multi-section emitting and receiving antennas which constitutes a practical realization of particular experimental scheme considered in Section 4. The EA and RA are composed from four and two sections, respectively, as it is shown in

Fig.5. The arrows mean directions of conduction currents at some given instant of time. Therefore, the symmetric form of multi-section emitting and receiving antennas implies no net current in radial directions. This property is important to reduce considerably undesirable electric dipole radiation in the case of EA and, in addition, to suppress any disturbing effect produced by electric dipole radiation in RA. Put in other terms, it provides us with a higher ratio of bound-to-radiation field strength (note that standard antennas are designed to reach the highest ratio of radiation-to-bound field strength in order to enhance the radiation). This circumstance is of crucial importance as concerns empirical observations of bound magnetic fields as well as the precision of measurements.

In respect to the approximation of quasi-stationary current, the use of multi-section antennas improves considerably the basic criteria $\frac{r}{c} \ll \frac{1}{\omega}$. In fact, all radial parts of each section make no contribution in generation of magnetic fields (bound or radiation) due to the cancelation of current flows in adjacent parts of neighbor sections. It stands out the role played by the arc fragment of every section, being thus the only part of the multi-section antenna capable to produce magnetic fields. Since the resultant magnetic field is determined entirely as a superposition of magnetic fields created by each section, then the applicability of the approximation of quasi-stationary current resides on its validity for each section. As a consequence, we can consider the criteria for the quasi-stationary current approximation of a multi-section antenna as:

$$\omega \ll \omega_c = \frac{nc}{r} \tag{18}$$

where ω_c denotes the critical value of the frequency of oscillations and n means the number of sections.

Thus, the use of multi-section type of antennas was fully justified in our approach by the above-exposed practical reasons. Let us now describe a technical realization of the experimental set-up as regards the emitting multi-section antenna (see Fig.6). A fast high-voltage spark gap (SG) constitutes the driving circuit of the EA and it is connected with the multi-section emitting circuit via the blocking capacitor C which also plays the role of the energy storage element. The whole circuit, presented in Fig.6, can be viewed as LC-contour with the proper frequency $\omega_0 = 1/\sqrt{LC}$, where L is the inductance of the EA. We also assume that the values of L, C and the radius r are given in the range of applicability of the approximation of quasi-stationary current, i.e. $\omega_0 \ll \omega_c$. The high-voltage supply (HV) is connected to the EA via the resistor R_f. The latter determines the time necessary to charge the capacitor C as well as the duration of the period in a series involving successive charges and discharges.

The magnitude of the initial current flow in the EA depends on the value of high-voltage U and the discharge time τ. The technical realization described above and presented in Fig.6, generally speaking, does not imply harmonic oscillations in the circuit of the EA. As a consequence, further on we shall assume the exponential character of the discharge process, i.e. $U(t) = U(0) \exp(-t/\tau)$ and the shape of the emitted signal will be conditioned by the Kirchhoff equation for the emitting circuit:

$$U_L + U_{R_e} + U_C = U(0)e^{-t/\tau} \tag{19}$$

10

where R_e is the characteristic resistance of the EA.

Taking into account standard relationships such as $U_L = L\frac{dI}{dt} = L\frac{d^2Q}{dt^2}$; $U_C = \frac{Q}{C}$ (where Q denotes the charge) and neglecting the resistance R_e (the approximation valid when forced oscillations take place), the Kirchhoff equation (19) takes the form:

$$\frac{d^2Q}{dt^2} + \omega_0^2 Q = Q_0 \omega_0^2 e^{-t/\tau} \tag{20}$$

where $Q_0 = U(0)/C$.

If one chooses the initial conditions $Q = Q_0$; $\frac{dQ}{dt} = 0$, the solution to Eq. (20) can be written as:

$$Q(t) = \frac{Q_0}{1 + \omega_0^2 \tau^2}(\cos\omega_0 t + \omega_0 \tau \sin\omega_0 t + \omega_0^2 \tau^2 e^{-t/\tau}) \tag{21}$$

providing also the time dependent magnitude of the conduction current $I(t)$:

$$I(t) = \frac{dQ}{dt} = \frac{Q_0 \omega_0}{1 + \omega_0^2 \tau^2}(-\sin\omega_0 t + \omega_0 \tau \cos\omega_0 t - \omega_0 \tau e^{-t/\tau}) \tag{22}$$

and its respective time derivatives:

$$\frac{dI}{dt} = \frac{Q_0 \omega_0^2}{1 + \omega_0^2 \tau^2}(-\cos\omega_0 t - \omega_0 \tau \sin\omega_0 t + e^{-t/\tau}) \tag{23}$$

$$\frac{d^2 I}{dt^2} = \frac{Q_0 \omega_0^3}{1 + \omega_0^2 \tau^2}(\sin\omega_0 t - \omega_0 \tau \cos\omega_0 t - \frac{1}{\omega_0 \tau}e^{-t/\tau}) \tag{24}$$

We are now in a position to approach a numerical evaluation of the output signal in the RA. Let the loops of the emitting and receiving antennas belong to the same plane xy as it is shown in Fig.7. The general expression (9) gives the resultant magnetic field **B** produced by the EA:

$$\mathbf{B} = \frac{1}{4\pi\varepsilon_0 c^2} \oint_{\Gamma} \left\{ \frac{[I]_v}{R'^2} + \frac{[\dot{I}]}{cR'} \right\} d\mathbf{l} \times \mathbf{n}_{R'} \tag{25}$$

where $R'_x = R + r\cos\theta - r_{EA}\cos\varphi$; $R'_y = r\sin\theta - r_{EA}\sin\varphi$; $R'_z = 0$; $d\mathbf{l}$ is an infinitesimal element of the emitting loop Γ and $\mathbf{n}_{R'} = \mathbf{R}'/R'$ is the unit vector.

The e.m.f. $\varepsilon(t)$ induced in the RA is due to the magnetic field **B** produced by the EA and can be calculated according to the integral form of the Faraday induction law:

$$\varepsilon = -\frac{d}{dt}\int_{S_{RA}} \mathbf{B}(R,t)\cdot d\mathbf{S} = -\int_0^{2\pi}\int_0^{r_{RA}} \frac{dB_z(R,t)}{dt} r\,dr\,d\theta \tag{26}$$

where S_{RA} and r_{RA} are the area and the radius of the RA, respectively.

Since we assume valid the approximation of quasi-stationary current, i.e. $\omega \ll \omega_c$, then at a given instant of time t the conduction current has nearly the same magnitude

11

$I(t)$ in all parts of the loop of the EA. Having this approximation in mind, we substitute (25) in (26) and find that:

$$\varepsilon = \frac{1}{4\pi\varepsilon_0 c^2} \int\limits_0^{r_{RA}} \int\limits_0^{2\pi} \int\limits_0^{2\pi} \frac{\left[\dot{I}\right]_v}{R'^3} \left(1 - \frac{r}{r_{EA}}\cos(\theta - \varphi) - \frac{R}{r_{EA}}\cos\varphi\right) r_{EA}^2 r\, dr\, d\theta\, d\varphi +$$

$$+\frac{1}{4\pi\varepsilon_0 c^2} \int\limits_0^{r_{RA}} \int\limits_0^{2\pi} \int\limits_0^{2\pi} \frac{\left[\ddot{I}\right]}{R'^2} \left(1 - \frac{r}{r_{EA}}\cos(\theta - \varphi) - \frac{R}{r_{EA}}\cos\varphi\right) r_{EA}^2 r\, dr\, d\theta\, d\varphi \qquad (27)$$

where the square bracket $\left[\dot{I}\right]_v$ means that the value of $\dot{I}$ in (23) is taken at the retarded time $t \to t - R'/v$ whereas the term $\left[\ddot{I}\right]$ implies the substitution $t \to t - R'/c$ in (24).

In order to bring our numerical evaluations as close as possible to the actual realization of the experiment, we also have taken into consideration the widths of the emitting and receiving antennas, denoted as h_{EA} and h_{RA} respectively. Thus, defining the current density per a unit length in the EA as I/h_{EA} we can rewrite (27):

$$\varepsilon = \frac{1}{4\pi\varepsilon_0 c^2 h_{EA}} \int\limits_0^{r_{RA}} \int\limits_0^{2\pi} \int\limits_0^{2\pi} \int\limits_0^{h_{RA}} \frac{\left[\dot{I}\right]_v}{R'^3} \left(1 - \frac{r}{r_{EA}}\cos(\theta - \varphi) - \frac{R}{r_{EA}}\cos\varphi\right) r_{EA}^2 r\, dr\, d\theta\, d\varphi\, dh +$$

$$+\frac{1}{4\pi\varepsilon_0 c^2 h_{EA}} \int\limits_0^{r_{RA}} \int\limits_0^{2\pi} \int\limits_0^{2\pi} \int\limits_0^{h_{RA}} \frac{\left[\ddot{I}\right]}{R'^2} \left(1 - \frac{r}{r_{EA}}\cos(\theta - \varphi) - \frac{R}{r_{EA}}\cos\varphi\right) r_{EA}^2 r\, dr\, d\theta\, d\varphi\, dh \quad (28)$$

where $R' = \sqrt{R_x'^2 + R_y'^2 + h^2}$.

The form of the calculated e.m.f. $\varepsilon(t)$ depends on the parameter τ which was introduced above as a parameter responsible for the duration of discharge processes in the circuit of the EA. In addition, we have taken into consideration the proper rise time of the RA (τ_{RA}) and the proper rise time of the oscilloscope (τ_o) in the circuit of the RA. It allowed us to use an effective rise time $\sqrt{\tau^2 + \tau_{RA}^2 + \tau_o^2}$ in order to make more realistic calculations concerning the front of the e.m.f. $\varepsilon(t)$ signal. For numerical calculations on base of the Eqs. (23)-(28) we used *Mathcad Professional 2000 software*. All necessary parameters as regards to the particular experimental settings, will be described in the next Section.

4 Experimental settings

The emitting multi-section antenna (see Fig.5a) was assembled according to the following geometric parameters: *(1)* the radius $r = 50mm$; *(2)* the width $h_{EA} = 50mm$ and *(3)*

the gap between adjacent sections - $3mm$. The frame of the EA was made of copper sheet with $1mm$ thickness. To deliver a current to every section simultaneously, we used four parallel cables, each one having the characteristic resistance of $50Ohms$ and the length of $20cm$. The inductance of the EA (all four sections are connected in parallel) is $L = 46 \pm 1 \ nH$. It was measured by the impedance meter $E7\text{-}14$ (Russia) at frequency $10kHz$.

To charge the RC circuit, we used a high-voltage supply of $U \leq 2kV$. The spark gap $EPCOS \ B88069\text{-}X3820\text{-}S102, \ A71\text{-}H10X \ 1400V/10A$ has a discharge voltage of $1.4kV$. Estimated discharge time of the RC circuit is $3ns$. The capacitor C has $22pF$, thus determining the proper frequency $\omega_0 = 1/\sqrt{LC} = 9.9 \times 10^8 \ s^{-1}$. However, the real measured frequency of current damped oscillations $(t \gg \tau)$ is $8.8 \times 10^8 \ s^{-1}$. It turned out to be a bit lower than the expected value ω_0 due to the presence of small proper circuit inductance and capacitance which are usually unknown. We found values $r = 50cm$ and $h_{EA} = 50$ to be optimal for the size of the EA. In this case, according to the definition (18), the critical frequency ω_c is $2.4 \times 10^{10} \ s^{-1}$, hence assuring the validity of the approximation of quasi-stationary current.

The capacitor C and the resistor $R_f = 5MOhms$ determine the duration of the period between discharges $T_d \approx 0.1ms$ which is important to exhibit the signal on the oscilloscope screen with due brightness. A synchronizing time signal was generated by the Rogovski belt[13], placed between the output of the discharge circuit and the input of the EA. The spark gap and the capacitor were kept inside the magnetic and electric shielding. It is also worth noting that a relative variation in amplitude of generated signals (caused by the instability of a threshold voltage in SG discharges) did not exceed 5% of the average value.

The geometrical parameters of the RA (see Fig.5b) are: (1) the radius $r = 50mm$; (2) the width $h_{RA} = 100mm$ and (3) the gap between adjacent sections - $3mm$. Both sections of this antenna are connected in parallel. Their frames are also made of copper sheet with $1mm$ thickness. The inductance of the RA, measured by the impedance meter $E7\text{-}14$ (Russia) at frequency $10kHz$, is $L = 49 \pm 1nH$. The proper rise time of the RA (coupled to the cable of $50Ohms$) can be estimated as $\tau_{RA} = \frac{49nH}{50Ohm} \approx 1ns$. We found values $r = 50cm$ and $h_{RA} = 100mm$ to be optimal for the size of the RA. The corresponding critical frequency $\omega_c = 1.2 \times 10^{10} \ s^{-1}$ is still one order of magnitude higher than the proper frequency of current oscillations ω_0, keeping the validity of the approximation of the quasi-stationary current for the RA.

To visualize signals generated in the RA, we used the oscilloscope $C1\text{-}108$ (Russia) with the time scale $1ns$ per division. The proper rise time of the oscilloscope is $\tau_o \approx 1ns$ and the expected time resolution is about $0.1ns$. Additionally, a maximal voltage sensitivity available by the oscilloscope is $0.01V$ per division. Both antennas were mounted on a wooden table and all metallic objects (with the capacity to reflect EM radiation) were removed from the experimental installations at distances exceeding $1.5m$. It assured to make observations in such a manner that during the period of the first $10ns$, all EM perturbations received by the RA could in no way be attributed to reflected fields.

5 Experimental measurements

We remind the reader that the *zero crossing method* (see Section 2) provides the type of variations $\Delta t(R)$ which are very sensitive to the particular value of the parameter v from the range $v \geq c$ and, therefore, it should be considered as a reliable empirical test of the applicability of the standard retardation condition ($v = c$) to bound fields. In Fig.8 we show the results of numerical calculations (for multi-section antennas) on the base of the Eqs. (23)-(28) as regards the assumption on the undefined parameter $v \geq c$ which was introduced to represent the spreading velocity of bound field components. Dot lines describe the time shift Δt dependence on the distance R between emitting and receiving antennas at the retardation conditions $v = c$; $v = 2c$ and $v = 10c$. The limit case $v = \infty$ we plotted in a continuous line. It is worth emphasizing that the types of numerical predictions for $v = c$ and $v = \infty$ are qualitatively in agreement with the predictions obtained in the case of an idealized magnetic dipole (see Fig.4).

Now we are in a position to apply the *zero crossing method* and to subject theoretical predictions $\Delta t(R)$ to empirical test. For this purpose, we placed the emitting and the receiving antennas in parallel positions as it is shown in Fig.7. Keeping the orientation of antennas unchanged, we varied the distance between them in the range of $R = 40 \div 200cm$, applying the step of $\Delta R = 20cm$. At each position we succeeded in producing detectable signals on the oscilloscope screen. In order to implement the *zero crossing method* (discussed in Section 3), we measured the instant t_{cross} when the oscillating disturbance crosses zero line for the first time. At short distances, the amplitude of the whole signal is large, hence providing the maximum steepness to the front of the signal. It allowed us to measure the value of t_{cross} with due precision (the estimated error was less than $0.1ns$).

To complete our measurements we had to obtain the information on the instant t'_{cross} when the reference signal (i.e. the harmonics of the type $\varepsilon_r = -\sin(\omega t - \omega R/c)$) crosses zero line for the first time. Since it cannot be done in direct measurements (the EA does not generate the reference signal alone), we proposed indirect but nevertheless unambiguous determination of the value of t'_{cross}. As it already has been stated, at large distances R^{-3}, R^{-2}-terms result negligible in comparison with the radiation R^{-1}-term. In fact, the numerical calculations based on Eq. (28) indicated that at the distance of $R = 200cm$ between the EA and RA, a relative contribution of both R^{-3} and R^{-2}-terms into the final signal is less than 0.1%. It means that at $R = 200cm$ there is practically no difference between the values of t_{cross} and t'_{cross} (here we remind a reader to see diagrams in Figs.2 and 3). Thus, the value of t'_{cross} once established at $R = 200cm$, can be easily recalculated for any $R < 200cm$. It provides us the reliable experimental evaluation of the difference $\Delta t = t_{cross} - t'_{cross}$ at each R from the range $R = 40 \div 200cm$. A graphic visualization of the empirically found dependence $\Delta t(R)$ we present in Fig.8 (black circles). The unexpected behavior of the experimentally found dependence $\Delta t(R)$ is strikingly evident and it is apparently at odd with the predictions of the standard EM theory (the dot line $v = c$).

14

6   Conclusions

Based on these results, one can conclude that empirical data unambiguously indicate on the non-applicability of the standard retardation constraint ($v = c$) to bound fields. Since the standard classical electrodynamics is generally acknowledged nowadays as the most orthodox example of a causal and deterministic classical field theory, one can suppose that the standard theory may contain certain (perhaps, empirically unverified) causal assumptions which go beyond what is fair to assume in the framework of the mathematical formalism. The first experimental indication on a difference between propagation velocity of bound and radiation fields can be regarded as an unexpected causal asymmetry in the structure of possible solutions to Maxwell's equations. The latter has no grounds in the formalism of the existing electromagnetic theory and implies that a possible interpretive framework can be wider than the standard account allows. In our opinion, the presence of this fundamental uncertainty in the classical EM theory is due to the fact that perhaps there has not been realized the considerable importance in careful drawing and empirical testing distinction between bound and radiation field components. Put in other terms, it has to imply a considerable shift of attention towards the conception of the velocity dependent (bound) components of EM field because they may result of a crucial importance in illuminating alternative foundations of the classical electrodynamics.

In this respect, advocates of alternative views may appeal to the fact that at the time of Hertz experiments on propagation of EM interactions there was already a consistent rival approach to electromagnetic phenomena that emphasized the distinction between spreading velocity of bound and radiation EM field components. In the history of physics it is regarded as Helmholtz's electrodynamics[14]. Moreover, Maxwell's equations appeared in Helmholtz's theoretical scheme in a limit when the spreading velocity of bound (electrostatic in Helmholtz's classification) electric components tended to infinity. In this case, the propagation velocity of radiation waves (electrodynamic components in Helmholtz's classification) resulted equal to the velocity of light as it was assumed in Maxwell's theory (for more details, see[6],[15]). Recently, the same conclusion on a possibility of essential difference between spreading velocity of bound and radiation EM field components was obtained in completely independent and mathematically consistent approaches to the classical electromagnetic theory based on Maxwell's equations[3],[16]−[17].

We also have to point out the fact of a nearly perfect coincidence between experimental data and theoretical predictions based on the Eq. (9) for the spreading velocity of bound fields highly exceeding the velocity of light ($v \gg c$). This circumstance can be considered as a strong indication on the validity of a new generalized Biot-Savart law in form similar to the Eq. (9) which differs form the generally accepted expression (8) only as regards the spreading velocity of bound components, i.e. the condition $v \geq c$.

Nevertheless, speaking in strict terms, any discrepancy of experimental observations with theoretical predictions made on the basis of the standard condition $v = c$ does not automatically imply the correctness of our hypothesis in form of the Eq. (9) but rather experimentally observed violation of the applicability of the standard retardation

condition to bound fields. By its significance and importance, this experimental fact may be comparable with the violation of Bell's inequalities in quantum mechanics. It is very likely that both manifestations of non-locality might have the same origin. Moreover, we are inclined to think that non-local characteristics of bound fields shed a new promising light on a possible close relationship between classical electrodynamics and quantum mechanics.

Having in mind the challenge of measuring very feeble effects produced by bound fields, we have introduced into experimental practice multi-section emitting and receiving antennas that are designed to rise substantially the ratio of bound-to-radiation field strength. However, our experimental experience led us to the conclusion that a direct measurement of the spreading velocity of bound fields still must be qualified as a rather difficult task even if one implements experimental facilities available in modern physics laboratories. In this respect, we would like to emphasize some technical circumstances of our experimental approach. Due to a rapid fall of bound field amplitudes as R^{-2} and R^{-3}, the range of variation ΔR of the distance between emitting and receiving antennas has been essentially restricted by approximately $1m$. If we consider EM waves travelling with the velocity of light c, the difference $\Delta R \approx 1m$ means the time shift $\Delta t = \Delta R/c \approx 3ns$. In order to achieve a necessary precision of measurements (within the time range of $3ns$), the front of a generated signal must not exceed the value of $1ns$, (i.e. $4ns$ for a period of one quasi-harmonic signal) which corresponds to the angular frequency $\omega = 1.5 \cdot 10^9 Hz$. Numerical calculations show that a typical size of antenna (emitting at the frequency $\omega = 1.5 \cdot 10^9 Hz$) is about several cm and, therefore, at small distances (for instance, $R \approx 0.1m$) comparable with the size of the EA, the amplitude of the output signal should be of the order of $1V$. The crucial parameter that is the ratio of bound-to-radiation field strength also falls down rapidly with the distance as approximately $\left(\frac{c}{\omega R}\right)^2$. In our experiments, this ratio is close to unity at $R \approx 0.2m$ and results negligible already at distances exceeding $1m$. Hence, if there is an intention to produce any observable separation of bound and radiation components at $R = 1m$, the value of the ratio of bound-to-radiation field strength has to be close to unity at this distance, i.e. one has to assume that $\omega \approx c/R = 3 \cdot 10^8 Hz$. It implies a considerable rise of the front of generated signals up to nearly $5ns$ which already will exceed the permissible time shift of about $3ns$, making impossible any visual distinction between bound and radiation contributions into the resultant signal.

Thus, at present stage these circumstances made it almost unattainable task to undertake direct measurements of spreading velocity of bound magnetic fields. Having in mind experimental facilities available at the time of Hertz's experiments (1886-1891), we might intuitively assume that the problem of propagation of electromagnetic interactions could hardly have been resolved definitely at the end of the 19th century in favor of one of the rival theories (Maxwell's or Helmholtz's electrodynamics). Nevertheless, in contrast to our possible reservations, Hertz's contemporaries accepted his experiments almost unconditionally, i.e. by the beginning of the 20th century the problem of propagation of electromagnetic interactions had been considered as definitely resolved. It gave a rise to the conviction that the standard retardation condition $(v = c)$ has a general validity for all components of EM field. In this respect, we stress again that Hertz's experiments

were not especially thought-out to test the applicability of the retardation condition to bound fields, since at the time of Hertz's experiments the classical electromagnetism had not yet been completed in its modern theoretical framework. Therefore, from the point of view of the modern EM theory, this fact implies a methodological incompleteness of Hertz's experimental approach. In our opinion, these historical circumstances combined with the extreme feebleness of the effects produced by bound fields deprived the majority of physicists (from the beginning of the 20th century up till now) of the interest towards experimental study of bound fields properties.

7 Acknowledgments

APPENDIX. Derivation of the value of magnetic field due to an idealized magnetic dipole under the general assumption $v \geq c$

First, it is worth reminding that Eq. (8) was obtained in[8] at the low velocity relativistic limit of the exact solution (6) of the D'Alembert equation (7) when the centripetal acceleration of the moving charges is ignored. The latter requirement implies that in places where the antenna loop is curved, the current flow $I(t)$ and the rate of time variation of current $\dot{I}(t)$ are parallel to the tangential direction along the loop. To illustrate the derivation of Eq. (10) from the hypothetical general case driven by Eq. (9), we shall use the same assumptions as it is done in[8] and follow the analogous procedure implemented in[9].

Thus, if the radius r of the loop of the antenna is negligible in comparison with the distance to the point of observation R, i.e. $r \ll R$, then the shape of the antenna has no importance and it can be chosen in a way to simplify theoretical calculations. So, let us consider the small current carrying coil $ABCD$ shown in Fig.9. The arrow indicates the direction of the flowing current. The sections AD and BC are arcs circles, with centers at the point of observation P. Both circles have the radius value R and $R + \delta R$ respectively, where $\delta R \ll R$. Thus, if the length of the section AD is equal to r (where $r \ll R$), then the length of BC is $r(1 + \delta R/R)$.

Let us now determine the magnetic field $\mathbf{B}$ at the point of observation P and at the time of observation t. According to Eq. (9) the contributions of the currents in the sections AB and CD are both zero since $\mathbf{k} \times \mathbf{n} = 0$. Thus, we can calculate the value of the magnetic field generated only by the sections BC and AD:

$$\mathbf{B} = \frac{1}{4\pi\varepsilon_0 c^2} \oint_{BC+AD} \left\{ \frac{[\not{I}]_v}{R^2} + \frac{\left[\dot{I}\right]}{cR} \right\} \mathbf{k} \times \mathbf{n} dl \tag{29}$$

17

Integrating Eq. (29) we obtain the value of the magnetic field generated by the section BC:

$$\mathbf{B}_{BC} = \frac{1}{4\pi\varepsilon_0 c^2} \left\{ [I]_v \frac{r(1+\delta R/R)}{R^2(1+\delta R/R)^2} + \left[\dot{I}\right] \frac{r(1+\delta R/R)}{cR(1+\delta R/R)} \right\} \mathbf{k} \qquad (30)$$

and by the section AD respectively:

$$\mathbf{B}_{AD} = -\frac{1}{4\pi\varepsilon_0 c^2} \left\{ [I]_v \frac{r}{R^2} + \left[\dot{I}\right] \frac{r}{cR} \right\} \mathbf{k} \qquad (31)$$

Since $\delta R/R \ll 1$, the use of the binomial theorem is justified and Eq. (30) takes a more compact form:

$$\mathbf{B}_{BC} = \frac{1}{4\pi\varepsilon_0 c^2} \left\{ [I]_v \frac{r}{R^2}(1 - \frac{\delta R}{R}) + \left[\dot{I}\right] \frac{r}{cR} \right\} \mathbf{k} \qquad (32)$$

The circumstance that the section AD is placed closer to the point of observation P means that any signal travelling with the finite velocity and produced in this section at some initial instant t_0 will arrive at the point P earlier than its BC counterpart, generated at the same time t_0.

Under the assumption $v \geq c$, bound components of the magnetic fields $\mathbf{B}_{BC}$ and $\mathbf{B}_{AD}$ arrive at the point of observation P with different values of retardation time $t' = t - (R+\delta R)/v$ and $t' = t - R/v$ respectively. Therefore, both values of current $[I]_v$ in (30) and (31) have been generated at different initial instants of time $t_0^{BC} = t - (R+\delta R)/v$ and $t_0^{AD} = t - R/v$, where t is the time of observation at P. The shift between t_0^{BC} and t_0^{AD} is $\Delta t_v = t_0^{AD} - t_0^{BC} = \delta R/v$. Both values $I(t_0^{BC})$ and $I(t_0^{AD})$ can be related if one knows the rate of change of current $\dot{I}$ in one of the sections:

$$I(t_0^{BC}) = I(t_0^{AD} - \delta R/v) = I(t_0^{AD}) - \dot{I}(t_0^{AD})\delta R/v \qquad (33)$$

The same reasoning is also applicable to the radiation components which will arrive at P with different values of retardation time $t' = t - (R + \delta R)/c$ and $t' = t - R/c$ respectively. The shift between corresponding values of retardation time is $\Delta t_{v=c} = t_0^{AD} - t_0^{BC} = \delta R/c$. By analogy with (33), it determines the following relationship:

$$\dot{I}(t_0^{BC}) = \dot{I}(t_0^{AD} - \delta R/v) = \dot{I}(t_0^{AD}) - \ddot{I}(t_0^{AD})\delta R/v \qquad (34)$$

Thus, Eq. (32) can be rewritten as:

$$\mathbf{B}_{BC} = \frac{1}{4\pi\varepsilon_0 c^2} \left\{ (I_0 - \dot{I}_0\frac{\delta R}{v})\frac{r}{R^2}(1 - \frac{\delta R}{R}) + (\dot{I}_0 - \ddot{I}_0\frac{\delta R}{c})\frac{r}{cR} \right\} \mathbf{k} \qquad (35)$$

where $I_0 = I(t_0^{AD}) = [I]_v$ and $\dot{I}_0 = \dot{I}(t_0^{AD}) = \left[\dot{I}\right]_v$ are evaluated at the retarded time $t' = t - R/v$ whereas $\ddot{I}_0 = \ddot{I}(t_0^{AD}) = \left[\ddot{I}\right]$ at $t' = t - R/c$.

Adding equations (35) and (31) we find the resultant magnetic field at the point P and the time t:

$$\mathbf{B} = \frac{\Delta S}{4\pi\varepsilon_0 c^2} \left\{ \frac{[I\!\!/]_v}{R^3} + \frac{c}{v}\frac{\left[\dot{I\!\!/}\right]_v}{cR^2} + \frac{\left[\ddot{I\!\!/}\right]}{c^2 R} \right\} \mathbf{k} \tag{36}$$

where we have taken into account that the area of the loop $ABCD$ is $\Delta S = r\delta R$.

Under the standard retardation constraint $v = c$ valid in respect to all components of the magnetic field, we arrive at the conventional form[9]–[12]:

$$\mathbf{B}(R,t) = -\frac{\Delta S}{4\pi\varepsilon_0 c^2} \left\{ \frac{[I]}{R^3} + \frac{\left[\dot{I}\right]}{cR^2} + \frac{\left[\ddot{I}\right]}{c^2 R} \right\} \mathbf{k} = -\frac{\mu_0}{4\pi} \left\{ \frac{[\mathbf{m}]}{R^3} + \frac{[\dot{\mathbf{m}}]}{cR^2} + \frac{[\ddot{\mathbf{m}}]}{c^2 R} \right\} \tag{37}$$

where $\mathbf{m} = I\Delta S\mathbf{k}$ and $\varepsilon_0\mu_0 = 1/c^2$.

References

[1] J.D. Jackson, *Classical Electrodynamics*, 2nd Edition (John Wiley, New York, 1975)

[2] L.D. Landau and E.M. Lifshitz, *The Classical Theory of Fields* (Addison-Wesley, Cambridge, Mass., 1951)

[3] A.E. Chubykalo and R. Smirnov-Rueda, *Phys. Rev. E*, **53** (1996) 5373

[4] R.A. Villecco, *Phys. Rev. E*, **48** (1993) 4008

[5] H. Hertz, *On the Finite Velocity of Propagation of Electromagnetic Action*, (1888) in "Electric Waves, Collection of Scientific Papers", (Dover, New York, 1962), p. 108

[6] R. Smirnov-Rueda, *Found. Phys.*, **35**(1) (2005) 1

[7] R.I. Tzontchev, A.E. Chubykalo and J.M. Rivera-Juarez, *Hadronic Journal*, **23** (2000) 401

[8] O.D. Jefimenko, *Electricity and Magnetism: An Introduction to the Theory of Electric and magnetic Fields*, 2nd Edition (Electret Scientific Co., Star City, WV, 1989)

[9] W.G.V. Rosser, *Interpretation of Classical Electromagnetism*, Fundamental Theories of Physics, Vol. 78, Edt. A. Van der Merwe (Kluwer Academic Publishers, Dordrecht/Boston/London, 1997)

[10] J.D. Jackson, *Am. J. Phys.*, **70** (2002) 917

[11] W. Tittel at al, *Phys. Rev. Lett.*, **81** (1998) 3563

[12] J.A. Stratton, *Electromagnetic Theory* (McGraw-Hill Book Co., New York-London, 1941)

[13] H. Knöpfel, *Pulsed High Magnetic Fields* (North Holland Publishing Co., Amsterdam/London, 1970)

[14] H. Helmholtz, *Wissenschaftliche Abhandlungen*, Vol.1 (Barth, 1882)

[15] J. Buchwald, *The Creation of Scientific Effects: Heinrich Hertz and Electric Waves* (The University of Chicago Press, Chicago, 1994)

[16] A.E. Chubykalo and R. Smirnov-Rueda, *Mod. Phys. Lett. A*, **12** (1997) 1

[17] A.E. Chubykalo and S.J. Vlaev, *Int. J. Mod. Phys. A*, **14** (1999) 3789
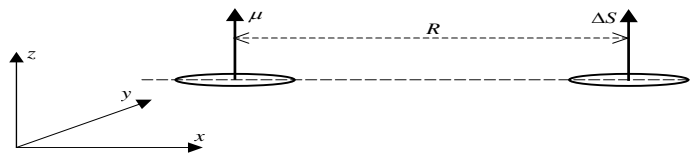
Figure 1: Geometrical configuration of the EA and RA in the plane xy

The signals ε_r and $\varepsilon_{(v=c)}$

ε_r

$\varepsilon_{(v=c)}$

The components of the signal $\varepsilon_{(v=c)}$

Δt_3 Δt_2 Δt_1 Far field zone $\Delta t = 0$

R^{-3}-term

R^{-2}-term

R^{-1}-term

$\Delta t = \varepsilon_{(v=c)} - \varepsilon_r$

π

Δt_3 Δt_2 Δt_1

Far field $R = ct$
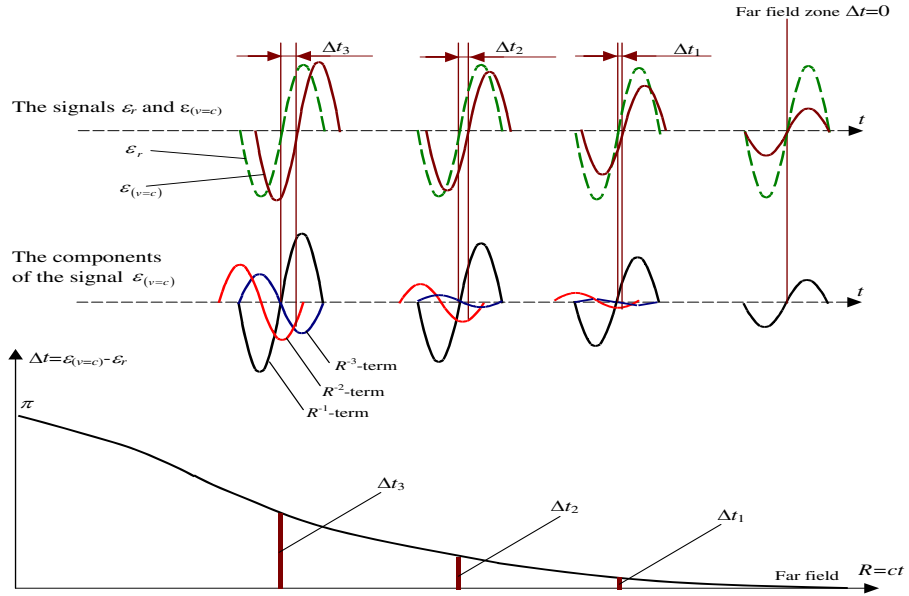
Figure 2: the case $v = c$; evolution (with R and t) of the temporal shift between $\varepsilon_{v=c}(t)$ and $\varepsilon_r(t)$; specification of the relative contribution of R^{-3}, R^{-2} and R^{-1}-terms into the resultant signal $\varepsilon_{v=c}(t)$; dependence $\Delta t(R)$ corresponding to the time shift between instants when signals $\varepsilon_{v=c}(t)$ and $\varepsilon_r(t)$ cross zero line

22

The signals ε_r and $\varepsilon_{(v=\infty)}$

$\Delta t>0$

$\Delta t<0$

The components of the signal $\varepsilon_{(v=\infty)}$

$\Delta t>0$

$\Delta t<0$

R^{-3}-term

R^{-1}-term

$\Delta t=\varepsilon_{(v=\infty)}-\varepsilon_r$
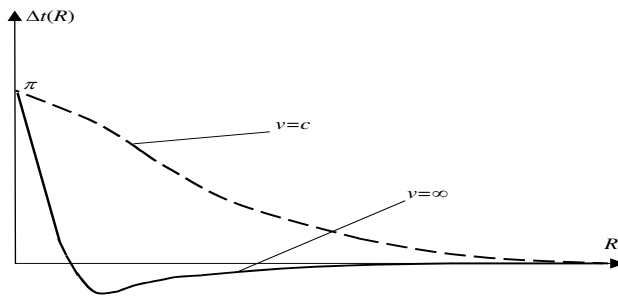
π

Far field

$R=ct$
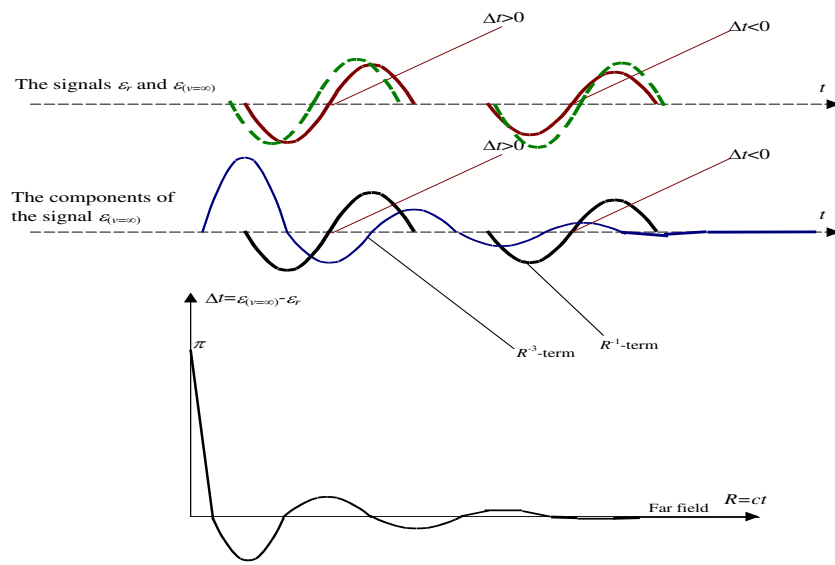
Figure 3: the case $v = \infty$

Figure 4: the case $v = \infty$; the dependence $\Delta t(R)$ is calculated under the assumption that the relative contribution of R^{-3}-term into the resultant signal $\varepsilon_{v=\infty}(t)$ is negligible in comparison with R^{-1}-term at distances $R > c/\omega$

emitting section

insulating holder

a)

receivinging section

insulating holder

b)
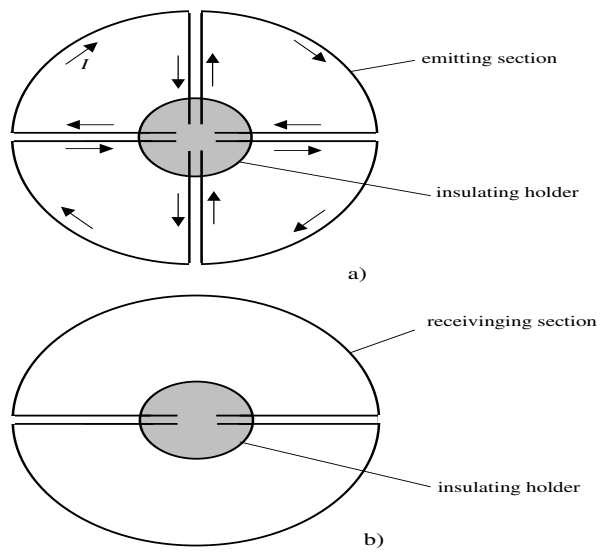
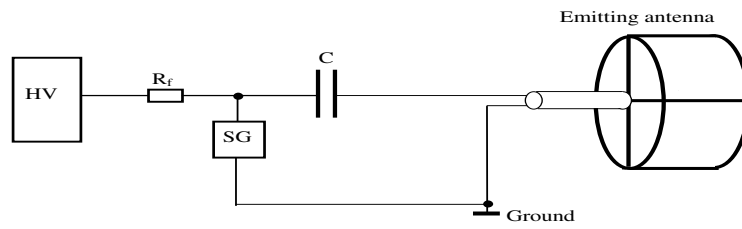Figure 5: *(a)* cross-section of the EA; the arrows show the direction of current flows in all sections; *(b)* cross-section of the RA.

Figure 6: Circuit of the emitting antenna.
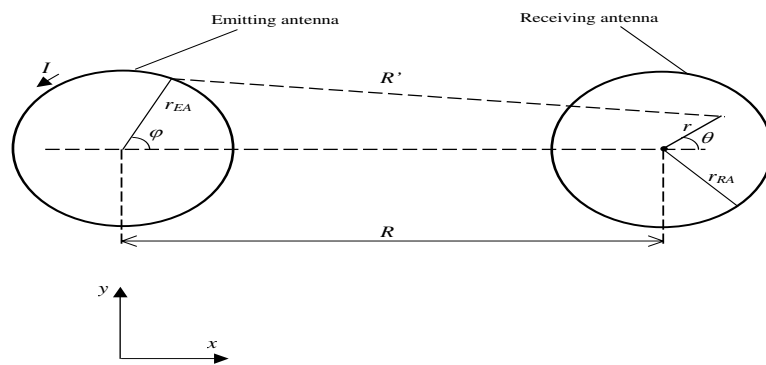
Figure 7: Calculation of the resultant magnetic field **B** and e.m.f. $\varepsilon(t)$ in the loop of the RA; specification of polar coordinate systems attached to the EA and RA.
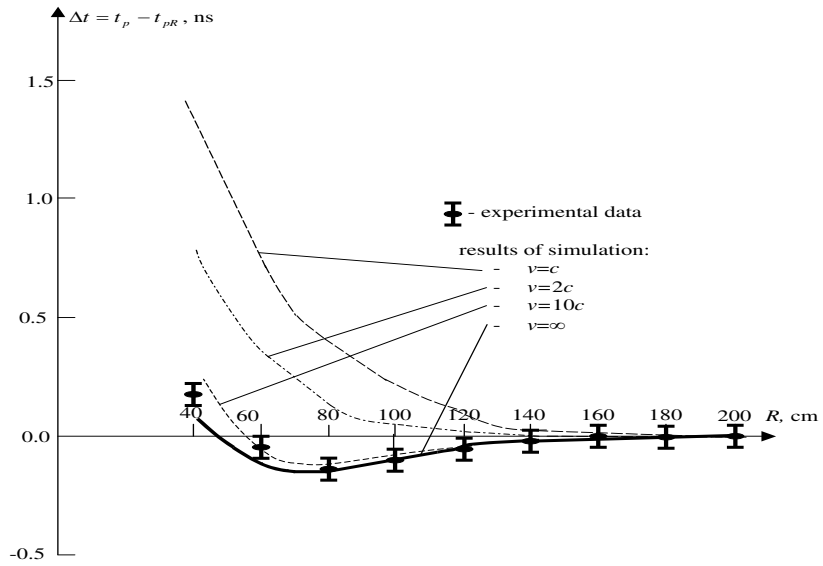
Figure 8: Dot lines illustrate numerical predictions of the dependence $\Delta t(R)$ for $v = c$; $v = 2c$ and $v = 10c$; continuous line corresponds to the numerical predictions of $\Delta t(R)$ for $v = \infty$; empirically found dependence $\Delta t(R)$ is represented by black circles.
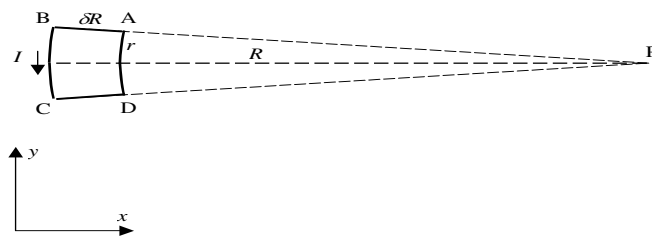
Figure 9: Calculation of the resultant magnetic field $\mathbf{B}$ at the point P due to both bound $\mathbf{B_u}$ and radiation $\mathbf{B_a}$ components generated by varying currents $I(t)$ in the loop $ABCD$